IOP Publishing | International Atomic Energy Agency Nuclear Fusion

Nucl. Fusion **58** (2018) 016009 (9pp) https://doi.org/10.1088/1741-4326/aa8bf4

Electromagnetic control of heat transport within a rectangular channel filled with flowing liquid metal

M. Modestov[1,2], E. Kolemen[2], A.E. Fisher[2] and M.G. Hvasta[2]

[1] Nordita, KTH Royal Institute of Technology and Stockholm University, 10691 Stockholm, Sweden
[2] Dept. of Mechanical and Aerospace Engineering, Princeton University, Princeton, NJ 08544, United States of America

E-mail: MHvasta@princeton.edu

Received 16 December 2016, revised 30 August 2017
Accepted for publication 12 September 2017
Published 6 November 2017

Abstract

The behavior of free-surface, liquid-metal flows exposed to both magnetic fields and an injected electric current is investigated via experiment and numerical simulations. The purpose of this paper is to provide an experimental and theoretical proof-of-concept for enhanced thermal mixing within fast-flowing, free-surface, liquid-metal plasma facing components that could be used in next-generation fusion reactors. The enhanced hydrodynamic and thermal mixing induced by non-uniform current density near the electrodes appears to improve heat transfer through the thickness of the flowing metal. Also, the outflow heat flux profile is strongly affected by the impact of the $J \times B$ forces on flow velocity. The experimental results are compared to COMSOL simulations in order to lay the groundwork for future liquid-metal research.

Keywords: liquid metal experiment, heat transport, MHD simulations

(Some figures may appear in colour only in the online journal)

1. Introduction

Despite considerable progress in magnetic fusion research, several fundamental problems still prevent fusion energy from being profitable or efficient. One of the main problems is first wall disruption under severe heat flux from the plasma. A flowing layer of liquid metal (LM) is an attractive alternative to solid tokamak interior walls [1, 2]. LM plasma facing components (PFCs) provide a robust, self-healing, heat removal method. However, the many engineering challenges associated with LM-PFCs require continued research. For this reason, the liquid metal experiment (LMX) at Princeton Plasma Physics Laboratory (PPPL) was designed to investigate heat transfer under a variety of flowing liquid metal operating conditions [3, 4].

During the LMX operation, a galinstan (GaInSn) flow is produced within a rectangular channel, as depicted in figure 1. The channel is 10.9 (cm) wide with a linear flow path length of approximately 100 (cm), and is situated within the air-gap of a C-shaped electromagnet. The electromagnet is capable of producing magnetic fields ranging from 0–0.3 (T) and generating a field that uniformly covers nearly 80 (cm) of the channel. Galinstan is pumped through the channel using a custom-built Archimedes style screw pump that can generate flows up to 3–4 (gpm) or ~11–15 (l min^{-1}). When the electromagnet is operating, two electrodes—one near the inlet and the other near the outlet of the channel—inject electric currents into the flow in order to generate a Lorentz force within the liquid metal. These electrodes are situated on the edges of the electromagnet in order to create a uniform current density within the liquid metal that is exposed to the uniform magnetic field. The range of LMX operating conditions can be found in table 1.

An array of thermocouples is situated below the channel with the sealed/sheathed thermocouple junctions penetrating approximately 1 (mm) through the base to take temperature measurements, as seen in figure 2. A rectangular 2.5 (cm) × 7.5 (cm) × 0.2 (cm) ceramic heater that operates at a constant 240 (W) is mounted to the channel lid just

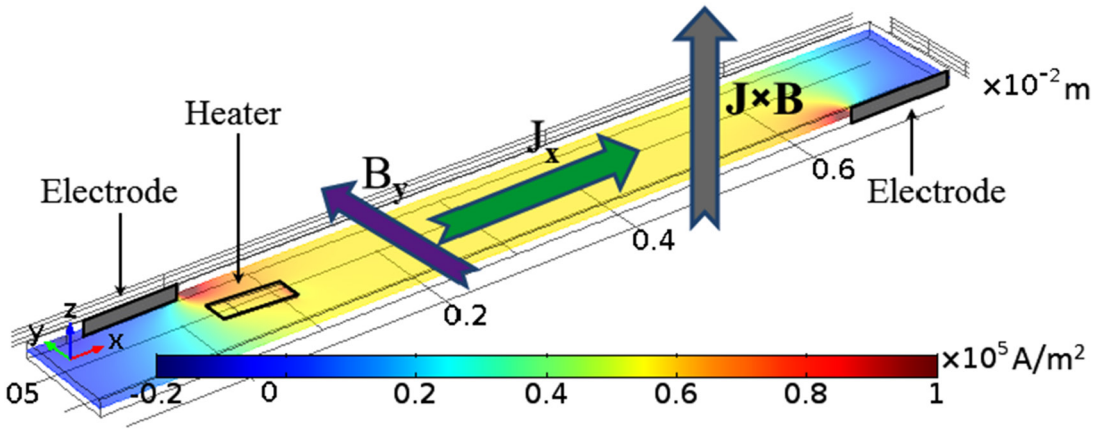

Figure 1. The numerical setup together with the typical current density distribution.

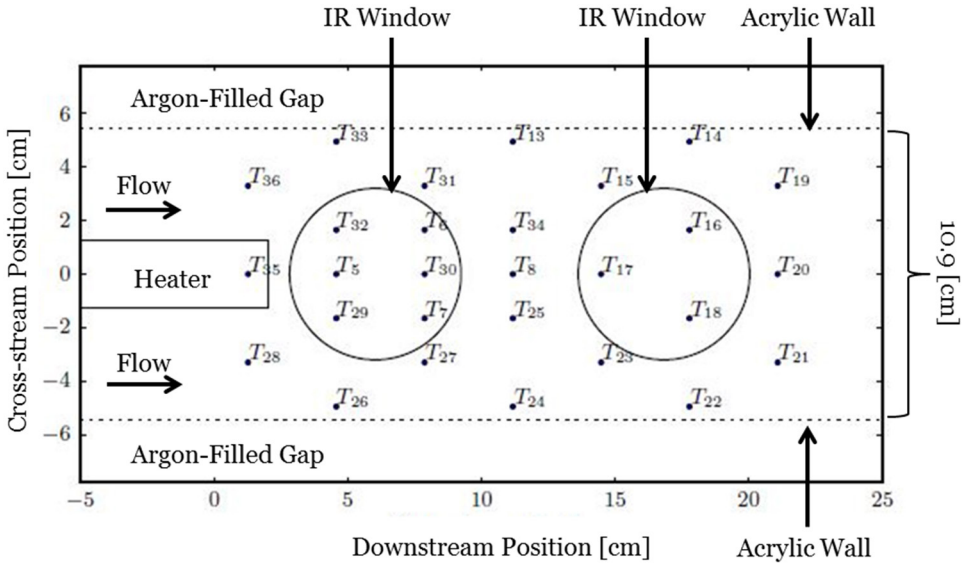

Figure 2. A schematic of the thermocouple array in LMX, with the heater and IR window positioning shown as the rectangle on the left and circles respectively. (Adapted with permission from [4].)

upstream of the thermocouples and angled into the flow so it can be used to provide a nearly constant heat flux into the liquid metal. In order to maintain a constant flow depth in the channel, a 0.6 (cm) weir was installed at the end of the duct. Approximately 7 (cm) upstream of the weir, a thermocouple was inserted into the flow and used to take the temperature measurements at the channel outlet.

Different flow parameters, such as height, velocity, Lorentz force, turbulence, etc., affect heat transport in different ways. However, it is difficult to determine the specific impact these individual parameters have on heat transport using only experimental thermocouple data because the data reflects the cumulative effect of all the different parameters combined. Therefore, proper MHD/CFD simulations that reproduce experimental heat transfer results are crucial to understanding the influence of particular flow parameters and disentangling the effects of various physical mechanisms [1, 5, 6]. The simulation of real tokamak physics on a full scale is still a numerical challenge; however, even simplified modeling allows scientists and engineers to understand the characteristic trends and dependencies. Additionally, numerical modeling could enable the extrapolation of the present results to the expected behavior in fusion reactors and the development of improved, reactor-relevant designs and control systems.

For successful operation of an LM divertor, numerous aspects must be thoroughly studied. The problem involves coupling between flow dynamics, heat transfer, electromagnetic interactions with conducting media, as well as free-surface flow phenomena. In this work, we are mostly interested in heat transport within the LM flows that are exposed to magnetic fields and externally applied electric currents. We discuss the experimental setup and the multiple effects of the resulting Lorentz force. For computer modeling we impose several simplifications; however, the numerical setup is very close to the LMX parameters. In the following sections we describe this problem in more detail and compare the simulation results with the experimental findings.

Heat transfer in liquid metal flows subject to MHD effects similar to those presented here have been studied by previous authors [7, 8]; however, the effect of externally injected electric currents on the generation of a Lorentz force perpendicular to the flow has not been thoroughly investigated.

Table 1. Non-dimensional numbers relevant to LMX operating conditions.

Non-dimensional #	Equation	Meaning	Range
Reynolds number	$\mathrm{Re} = \frac{u\rho h}{\mu}$	Ratio of inertial force to viscous force	2000–4000
Magnetic Reynolds number	$\mathrm{Re_m} = \frac{uh}{\sqrt{\mu_0\sigma}}$	Ratio of magnetic advection to magnetic diffusion	0.001–0.01
Hartmann number	$\mathrm{Ha} = Bh\sqrt{\frac{\sigma}{\mu}}$	Ratio of electromagnetic force to viscous force	0–140
Interaction parameter	$N = \frac{\mathrm{Ha}^2}{\mathrm{Re}}$	Ratio of electromagnetic force to inertial force	0–5

2. Governing equations and numerical setup

This paper focuses on the numerical simulations of LMX [3, 4]. Of particular interest is the electric current running through the flowing liquid-metal within an external magnetic field and the influence of the resulting Lorentz force upon the heat transport and general behavior of the flow. The goal of the simulations is to understand and reproduce the experimental LMX results; however, there are several aspects inherent to the experiment which are not included in the numerical model. The LM is described as an incompressible, electrically conductive fluid, accounting for its viscosity and thermal properties. The governing equations are the following:

$$\begin{gathered}\rho\frac{\partial \boldsymbol{u}}{\partial t} + \rho\left(\boldsymbol{u}\cdot\nabla\right)\boldsymbol{u} + \nabla p = \mu\nabla\cdot\left[\nabla\boldsymbol{u} + \left(\nabla\boldsymbol{u}\right)^T\right] + \boldsymbol{J}\times\boldsymbol{B}\\ \frac{\partial T}{\partial t} + \left(\boldsymbol{u}\cdot\nabla\right)T = \alpha\Delta T\\ \nabla\cdot\boldsymbol{u} = 0\\ \boldsymbol{J} = \sigma\left(-\nabla V + \boldsymbol{u}\times\boldsymbol{B}\right)\end{gathered} \tag{1}$$

where ρ is the LM density (6360 kg m^{-3}), u is the flow velocity, p is the hydrodynamic pressure, μ is the dynamic viscosity (0.002 71 Pa-s), J is the current density, B is the magnetic field, T is the temperature, V is the electric potential, α (1.497×10^{-5} m^2 s^{-1}) is the thermal diffusivity, and σ is the electric conductivity (3.15×10^6 S m^{-1}). The gravity term is omitted, as it is uniform in space and has no effect on this non-free-surface modeling. Equation (1) has been simulated with the help of the COMSOL Multiphysics software package. The solver is based on the finite element approach, aiming for easy coupling between different physics. It should be mentioned that the problem is three dimensional, as the magnetic field, the current density and the resulting Lorentz force are orthogonal to each other, as shown in figure 1.

LMX generates a free-surface flow of liquid metal known as 'galinstan' [9] in a horizontal rectangular channel constructed with insulating, acrylic walls. There is a resistive (ohmic) heater that is partially submerged into the fluid from the top of the flow [3, 4]. Two electrodes located on the opposite side walls inject electrical currents through the flowing galinstan. For the purposes of numerical modeling several useful simplifications, which are reasonable for the moderate parameters found within LMX, have been used to save computational time.

First, the fluid density is assumed to be constant, neglecting LM thermal expansion and omitting natural convection phenomena. In a fusion reactor these effects must be taken into account; however, under LMX conditions small temperature variations are not enough to cause noticeable density changes ($T_{\mathrm{Heater}} - T_{\mathrm{LM}}$ ~ 30 (K)). The heater position at the top of the flow diminishes the role of convection as well. Similarly, fluid transport quantities such as viscosity, thermal and electrical conductivities are also taken as constant with respect to temperature. For larger heat loads relevant to the reactor conditions, their temperature dependencies should be included. Second, ohmic heating within the galinstan caused by the injected electrical currents has also been omitted from the model, as it produces a much smaller temperature rise than the heater. The magnetic field is assumed to be constant in time and space, namely $B = (0, B_y, 0)$. For the larger part of the flow, the field variation is negligible; however, in the experiment the electromagnet is shorter than the channel length, so that there are small fringing effects near the inlet and outlet. Finally, LMX represents a free-surface flow, which under a relatively strong Lorentz force leads to an unstable and wavy flow surface. In the simulation setup we have a flat surface for the top wall with a slip boundary condition. Presumably this is the strongest simplification in the modeling. The real free-surface flow of the conducting media remains a serious numerical task even today.

Other boundaries are set as non-slip except for the constant velocity at the inlet (left channel side) and outlet boundary condition on the right channel side; at the inlet the temperature is set to a certain fixed value that is consistent with the experimental setup. The heater surface facing the channel provides heat flux with a constant power supply, so that the heater temperature varies depending on its surface area and the flow velocity; other walls are thermal insulators. Also, in the experiment the heater is held at a slight angle (~4°) with respect to the horizontal flow surface to minimize flow obstruction and provide thermal contact for a range of depths. In the simulation we use a similar setup, with the inclined heater being partially immersed in the liquid metal such that different flow heights result in a correspondingly different thermal contact areas. (In past work on LMX an analytical energy balance has been performed on the heater system, and it was found that the vast majority (~97%) of the power input goes into the flowing liquid metal regardless of the changes in flow height [4].)

The electric current density is computed due to the voltage difference boundary conditions set at the electrodes (shown in figure 1); the other walls are set as insulators as the experimental channel has an insulating acrylic liner. The choices for these boundary conditions were based on experimental observations and material properties. COMSOL is equipped with a physics-based meshing tool that was used to generate the mesh for these simulations. The meshing at the boundaries

was non-orthogonal, and the mesh resolution was chosen such that finer mesh studies yielded no significant differences in results and the convergence criteria were met. COMSOL has historical success in modeling MHD flows with these tools, and similar problems have been solved against widely agreed upon results for validation [10].

For diagnostics, the experimental setup provides measurements of the flow rate and surface height of the liquid metal. The temperature at the bottom of the channel is measured using multiple thermocouples (see figure 2). Hence, our simulation setup closely approximates the real experimental system, and takes into account the actual galinstan properties used in LMX [9].

3. Lorentz force effects in LMX

A major purpose of the current LMX configuration is to study the impact of the Lorentz force on the heat transfer in LM as well as its general influence on the flow. From our preliminary studies and theoretical expectations it has been found that the Lorentz force affects the flow in many ways. First of all, the $J \times B$ term is aligned with the z-axis, acting as 'effective gravity', which, under free-surface flow, modifies the flow height and velocity. As a result, this effect changes the heater contact area with the LM. Secondly, the experimental magnetic field covers most of the channel uniformly; however, there are two minor parts of the channel outside the electromagnet. This means that the downward force spatially varies in different parts of the channel, creating corresponding changes in the LM height. This results in an unstable and wavy flow surface which may cause additional mixing. This feature is not captured in our simulations and can cause discrepancies with the experimental results. Another issue deals with the specific location of the electrodes at the sides of the channel. As shown in figure 1 such a configuration yields non-uniform current density, producing larger magnitudes near the electrodes. This generates localized secondary flows that enhance LM mixing under the heater and closer to the outlet region.

Each of these aspects mentioned above deserves a separate detailed investigation. Below we present our simulation results and find out which of these factors prevails in heat transfer. The most important non-dimensional parameters for this problem are the Reynolds number, the magnetic Reynolds number, the Hartmann number and the interaction parameter as listed in table 1. The Reynolds number was approximately 4000 based on the flow depth and mean velocity, while the magnetic Reynolds number was a low 0.003. The Hartmann number and interaction parameter were approximately 140 and 5 respectively, making each one significantly lower than the expected reactor operating conditions.

3.1. Lorentz force as 'effective gravity'

We start our numerical investigations with a simpler but fundamental problem, studying the influence of flow height upon the heat transfer properties within a flowing LM. This is motivated by the fact that significant flow height changes have been observed in experiments due to the $J \times B$ force.

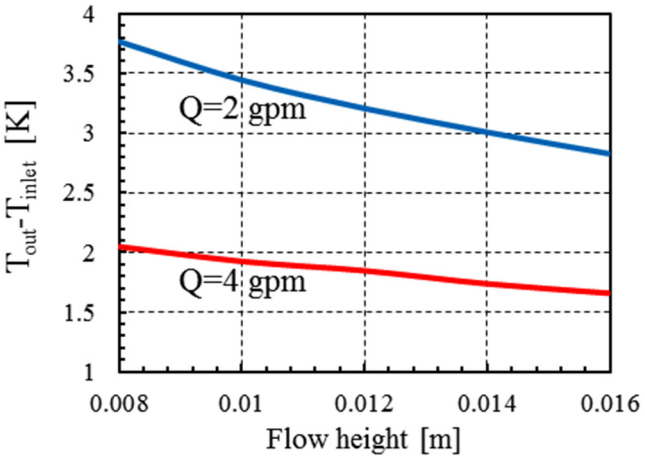

Figure 3. The bottom temperature dependence versus the flow height for two flow rates: $Q = 2$ gpm and $Q = 4$ gpm.

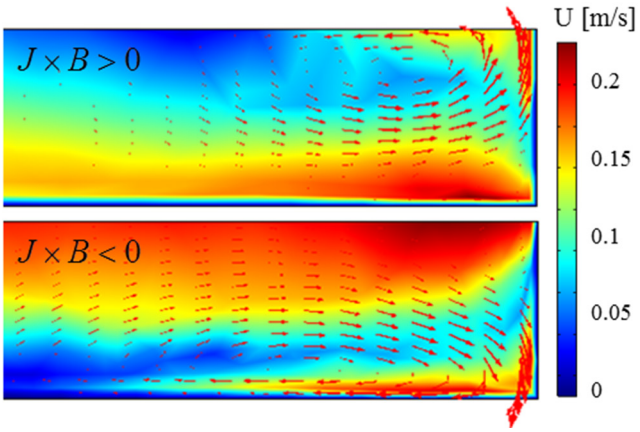

Figure 4. The velocity field at the y-z cross section near the electrode (at the right side) for two directions of the $J \times B$ force. The background stands for the total velocity magnitude, the vector field reflects the $(u_y;u_z)$ velocity components.

The latter can be considered as effective gravity, and under typical experimental conditions with $B_y \approx 0.3$ (T) and $J_x \approx 10^5$ A m^{-2} the magnitude of the resulting force reaches approximately half that of the gravitational forces on the Earth. Hence, the effective gravity varies from $\approx 0.5\,g$ to $\approx 1.5\,g$, where $g = 9.8$ m s^{-2} is the standard gravitational acceleration. For a free-surface flow, the gravity variation leads to a corresponding change in height, which can be estimated in a similar way as the hydraulic jump phenomena. Due to mass conservation, the flow velocity changes with height as well. Each of these two flow parameters has a strong influence upon heat transport in the liquid metal. In 3D geometry, rough analysis yields the h^{-3} dependence of the bottom temperature against the flow height and the u^{-2} dependence against the flow velocity. At the same time, for a fixed flow rate, the velocity is inversely proportional to the flow height, $u \sim Q/h$ where Q is the flow rate, so we expect a decrease of the bottom temperature with an increase of the flow height. In the experiment, the flow height varies from 9–16 (mm) when $B_y \approx 0.3$ (T) and the injected current densities range from $J_x \pm 10^5$ A m^{-2}.

In order to study the height effect on the heat transport we exclude the electro-magnetic physics from the model and

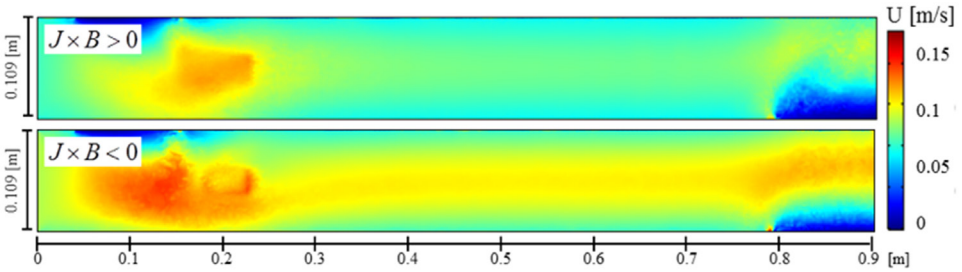

Figure 5. The velocity distribution taken at the middle of the channel height.

perform a set of simulations at a fixed flow rate varying the flow height only, imitating only one aspect of the $J \times B$ effect. For this setup, the contact area with the heater also remains constant. In figure 3 we present the liquid metal temperature taken at the bottom center of the outlet versus the flow height. Simulations have been performed for two different flow rates; the height variation and the flow rate are similar to the experimental values. The larger flow height corresponds to the upward direction of the $J \times B$ force and effectively decreases gravity; the smaller height values result from a downwards Lorentz force. This figure shows the temperature decrease with the flow height growth as would be expected, as the heat must travel to the bottom of the channel. The larger flow rate also decreases the bottom temperature, demonstrating the dependence on flow velocity. Based on figure 3 we may assume that the downward $J \times B$ force decreases the flow height with a corresponding increase of the bottom temperature. In the opposite case, the upward $J \times B$ force reduces the effective gravity, so that the flow becomes thicker and slower, while the channel bottom is exposed to lower temperatures. It should be noted that these simulation results cannot be compared directly to experimental measurements where a given flow rate produces a specific flow height and velocity. However, physically different flow heights can be obtained with different heights of the outlet weir.

3.2. Non-uniform current density and secondary flows

In its present version, LMX is equipped with two electrodes located at the sides of the channel as shown in figure 1. The current density exhibits uniform distribution in the main part of the channel, which in combination with the transverse magnetic field, B_y, produces a uniform force in the vertical direction. However, near the electrodes there is a concentration of electric current density. Hence, locally we obtain a stronger force directed upwards or downwards depending on the direction of the applied current. In real free-surface flow, it destabilizes the flow surface and may also enhance mixing. In our simulations the top boundary is kept fixed and flat. Nevertheless, one can easily see the action of this localized force by the velocity field presented in figure 4 at the cross-section of the channel in the y-z plane near one of the electrode edges. The vector field shows strong motion in the vertical direction near the electrode, generating secondary flow across the channel. The flow patterns are not completely symmetrical due to different boundary conditions at the bottom (non-slip) and top (slip) boundaries. The local peak of the $J \times B$ force

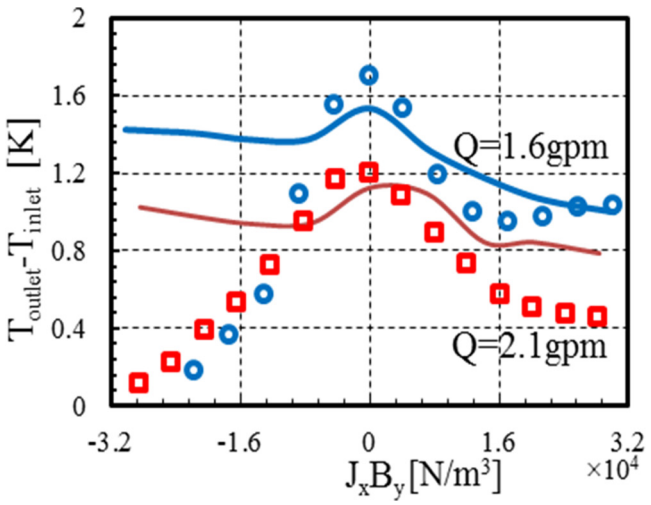

Figure 6. A comparison of the experimental outflow temperature measurements (markers) with the simulation results (solid lines) for two flow rates and various $J \times B$ forces.

eventually decays when moving from the electrodes to the channel center, where the force becomes uniform.

It is important to notice that this secondary flow is strong enough to modify the overall flow structure, playing the role of an invisible obstacle, which can be controlled or varied. This can already be seen in figure 4 where the modified background color indicates significant velocity variation within the flow.

This is demonstrated more clearly in figure 5 by the velocity distribution along the channel at the x-y cross-section taken at the middle channel height. The electrode-obstacle effect is revealed by the almost zero velocity near the electrode areas, and asymmetrical flow structure with respect to the central line of the channel. It should be mentioned that similar flow divergence near the electrodes has also been observed in experiments. The velocity increase in the middle of the channel close to the left electrode is due to the heater, which is partially immersed in the fluid suppressing the flow. The slight difference in velocity magnitude for different directions of the $J \times B$ force follows from the height variation at a constant flow rate setup. It is important to notice that specific electrode locations should have a large impact on the experimental results. One of the electrodes is located near the heater, hence it should enhance mixing under the heater affecting heat transfer efficiency. The second electrode is located near the outlet boundary where the outlet temperature measurement takes place.

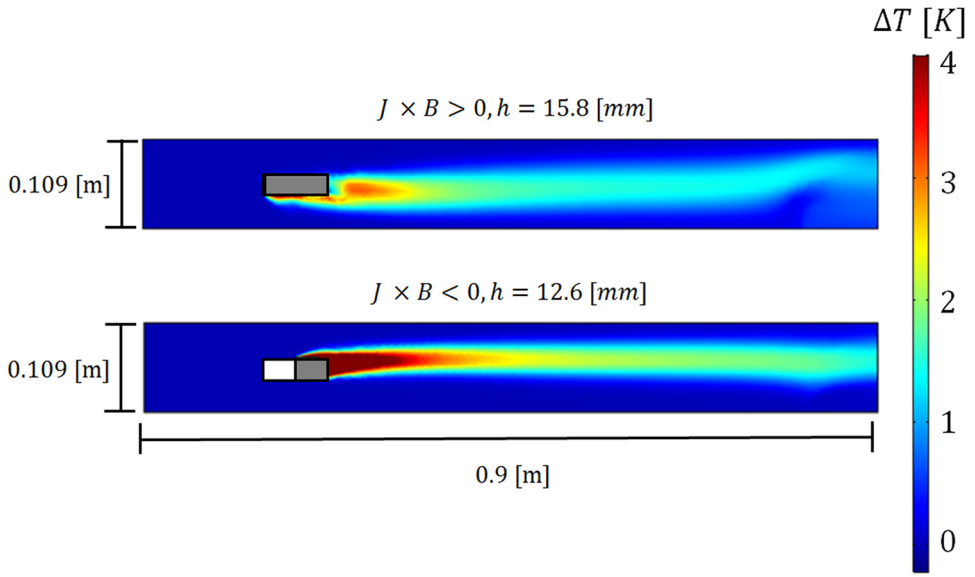

Figure 7. The temperature changes at the surface of the flowing liquid metal for two directions of the $J \times B$ force. In this figure, the submerged portion of the heater is colored gray while the heater in the plane of the fluid surface is colored white. (Flow directed from left to right.)

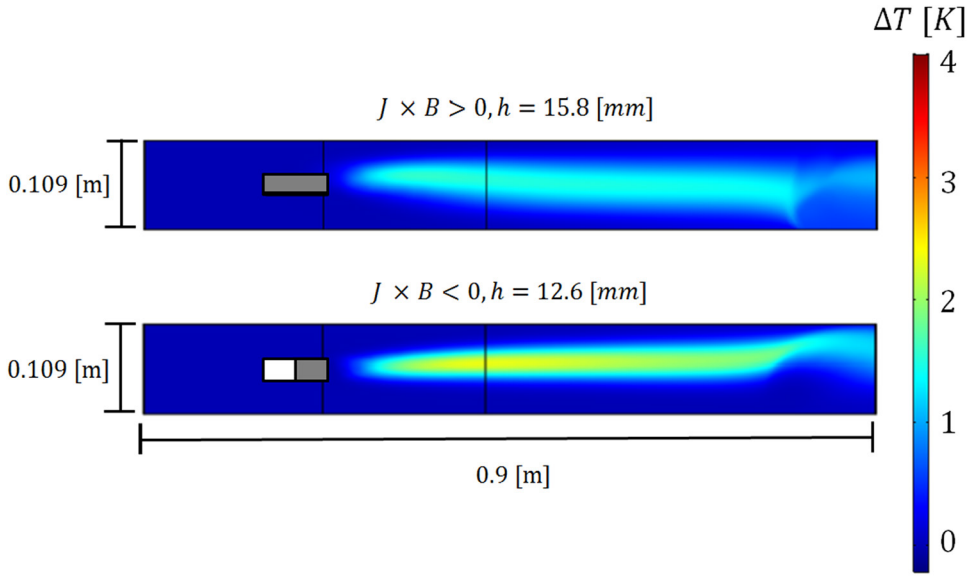

Figure 8. The temperature changes at the bottom of the LMX channel for two directions of the $J \times B$ force. In this figure, the submerged portion of the heater is colored gray while the heater in the plane of the fluid surface is colored white. (Flow directed from left to right.)

4. Simulations versus experiment

Finally, we perform a series of simulations taking into account several effects reflecting more relevant LMX operating conditions. The flow height is adjusted by the electric current amplitude according to the experimental height measurement. The heater position is bounded to the channel bottom so its thermal contact area changes with respect to the height of the fluid. The MHD drag is accounted for by varying the flow parameters for different magnetic fields.

The purpose of this simulation is to study heat transport in liquid metal and the temperature distribution in the channel. The temperature is experimentally measured by a set of thermocouples, providing accurate values at specific places. This data is easy to compare with the numerical simulation results. Still, real experiments involve several interplaying phenomena, such as heat transfer, the LM interaction with electric and magnetic fields, proper boundary layer formation and others that may not be completely accurately captured by COMSOL. For these reasons, together with the above simulations, it is challenging to expect perfect agreement between the simulation results and experimental data.

In figure 6, we present a comparison for the outlet temperature obtained from the simulations and provided by LMX. As the temperature increase due to the heater is quite moderate we depict the difference of the heated liquid metal temperature and the inlet temperature. The two sets of points and curves correspond to two flow rates; the data is obtained for

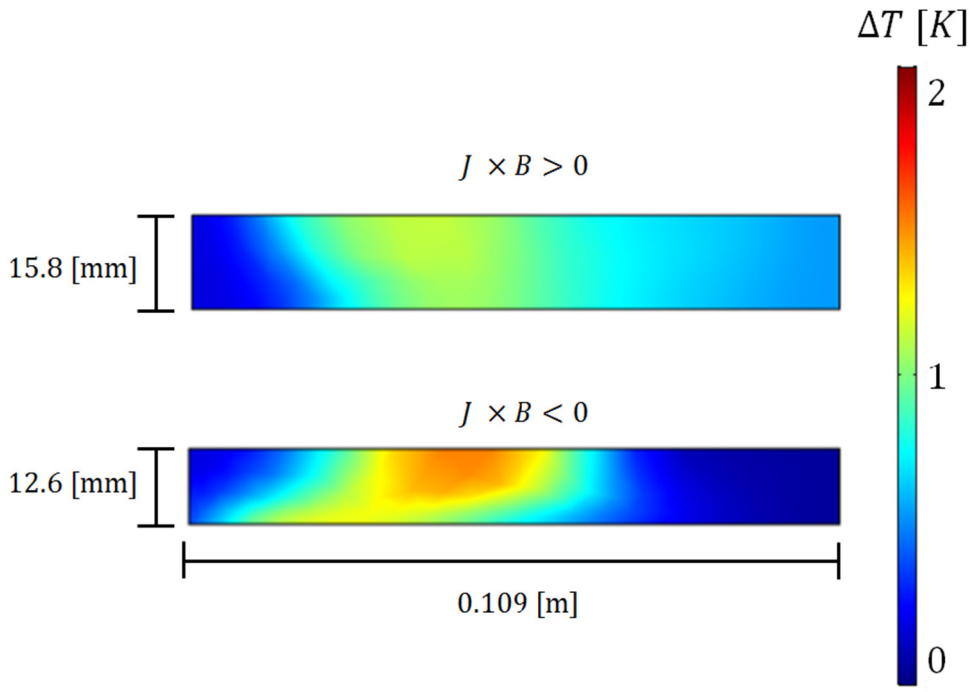

Figure 9. The temperature changes at the outlet for two directions of the $J \times B$ force. (Flow directed into the page.)

a magnetic field $B_y \approx 0.3$ (T) and a variable electric current magnitude. Despite noticeable differences between the experimental markers and the simulation curves, we should note close absolute values of the temperature differences. Moreover, both results demonstrate similar peaks at small currents. In addition to this, there are comparable trends for the positive (upwards) $J \times B$ force, which correspond to a thicker flow. Large discrepancies at a stronger negative $J \times B$ force may indicate the influence of the unstable free-surface or other effects which have not been captured in our simulations. We may also notice that the simulation curves exhibit the general trend depicted in figure 3.

The impact of different $J \times B$ forces can be seen in the temperature distributions presented in figures 7–9 which show the surface, bottom and outlet temperature changes respectively. As seen in these figures, in addition to $J \times B$ effects, the hydrodynamic interaction between the heater and the fluid also affects heat transport. For these simulations it was assumed that all of the heat flux entered the liquid metal from the underside of the heater. The resultant temperature changes look similar, although the Lorentz forces directed upward (against gravity) produce a larger temperature dispersion on the surface and bottom of the liquid metal. In this case, the higher temperature profile is wider than the one for the downwards force; the maximal temperature varies as well. We can also see the influence of the 'electrode-obstacle' that is caused by the non-uniform injected current density. This 'electrode-obstacle' leads to non-symmetric heat spreading with respect to the center-line of the channel. Closer to the outlet, one observes the apparent flow deviation near the electrode edge, where the electrical current density increases significantly. In this sense, the temperature distribution follows the velocity field depicted in figure 5. The outlet temperature

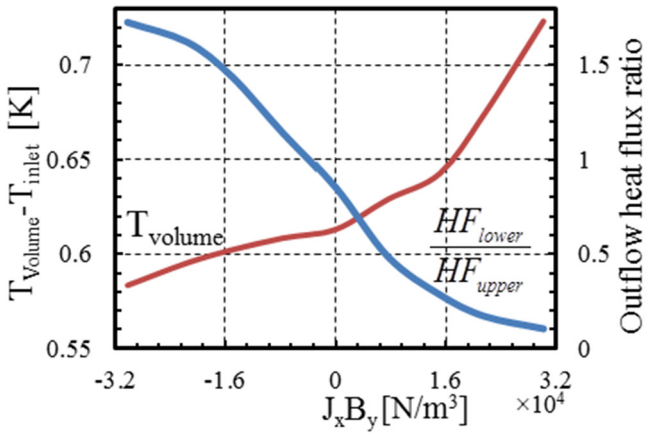

Figure 10. The increase in the total volume temperature and heat flux ratio at the outlet (lower to upper parts) against the $J \times B$ force acting in the experiment.

reveals similar distinctions to the surface and bottom temperature distributions. It is important to notice that the location of the maximum temperature shifts from the center due to the non-uniform electrical current density near the electrode. This may imply a larger discrepancy in the numerical and experimental results at larger Lorentz forces, as the experimental measurements were taken in the middle of the outlet region. Consequently, any distinction in the setups, like the poor electrical isolation of the inner channel blanket, may lead to noticeable change in the flow pattern and hence different measured temperatures.

A few more interesting effects of the Lorentz force are plotted in figure 10. Along the left axis we present the variation of the LM temperature averaged over the whole channel volume versus the Lorentz force. The absolute variation of this

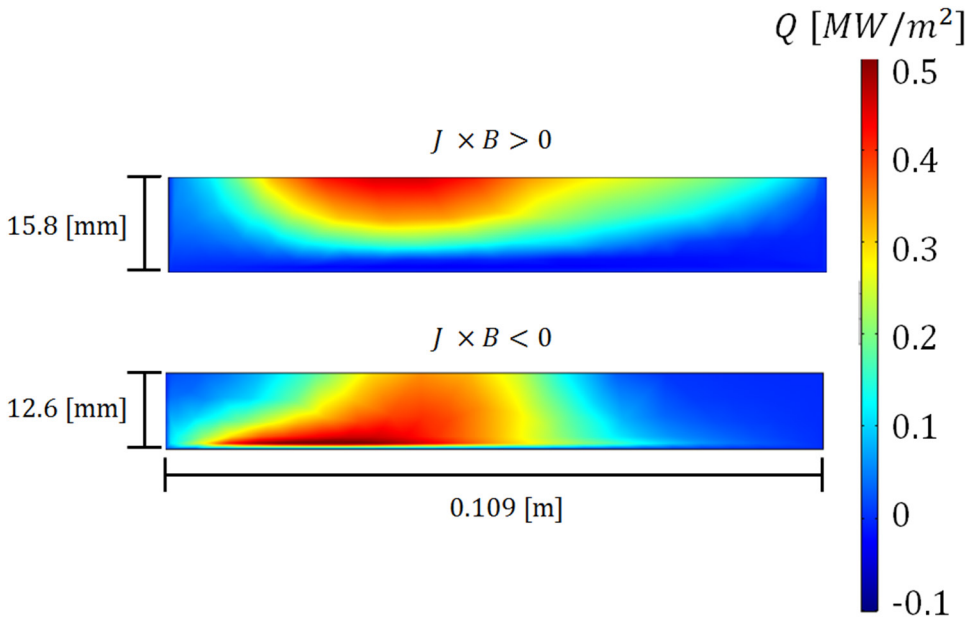

Figure 11. The heat flux ($Q = \rho c_p u_x \Delta T$) distribution at the outlet boundary. For this study $c_p = 365$ J kg^{-1} K^{-1}. The negative heat flux values correspond to the flow reversals ($u_x < 0$) caused by non-uniform current densities near the electrodes. (Flow directed into the page.)

temperature is small; however, relative change reaches 25%–30% for different directions of the electromagnetic force, which might be important for higher heat loads. Presumably, this temperature growth can be attributed to the enhanced heat transfer demonstrated in figures 7–9, where the upwards $J \times B$ force leads to more uniform heat transport through the liquid metal. On the right axis of figure 10, we plot the ratio of the heat flux through the outlet; $\mathrm{HF}_{\mathrm{lower}}$ corresponds to the averaged heat flux through the lower part of the outlet, $z \leqslant 0.5h$, where h is the flow thickness, and $\mathrm{HF}_{\mathrm{upper}}$ is computed for $z \geqslant 0.5h$. This heat flux ratio is clearly reflected in figure 11, where we show the distribution of the heat flux at the outlet. This reveals a large difference between the two cases. For this simulation, when the Lorentz force is directed downwards (parallel to gravity) most of the heat is directed towards the bottom of the channel. When the Lorentz force is directed upwards (antiparallel to gravity), high temperature galinstan moves near the top surface. Such distributions arise from the corresponding different velocity fields, occurring due to the secondary flow and non-uniformities near the electrodes.

5. Conclusions

The role of electromagnetic forces in thermal transport for LM has been studied by combining experimental results with numerical simulations. We discussed multiple possible effects of the $J \times B$ force and concluded that additional flow mixing induced by the non-uniform current density plays a dominant role in the present heat transfer experiments. On the one hand, the upward $J \times B$ force within the LMX intensifies mixing, but it also concentrates most of the heat flux in the upper layers of the flow, which might lead to possible LM evaporation or heat radiation from the surface in real tokamak applications. On the other hand, for this work, the downwards Lorentz force shifts the heat flux to the bottom of the channel, making heat removal more uniform through the thickness of the flowing liquid metal.

Additional investigations are needed to understand the discrepancy between the numerical and experimental results, as well as to realize the most efficient divertor design for tokamak applications. Strong variation of the outflow heat flux due to the Lorentz force action encourages further research in this field. The detailed mechanism and optimal current configuration has not been fully understood, although it is clear that the electric current running through the LM could be used to control the uniformity of the heat distribution in the conducting fluid.

Acknowledgments

M. Modestov acknowledges the Swedish Research Council (VR) for the International Postdoc grant no. 637-2014-465.

The research described in this paper was conducted under the Laboratory Directed Research and Development Program (LDRD) at Princeton Plasma Physics Laboratory, a national laboratory operated by Princeton University for the US Department of Energy under Prime Contract Number: DE-AC02-09CH11466.

The digital data for this paper can be found at: http://arks.princeton.edu/ark:/88435/dsp01x920g025r

References

[1] Morley N.B. *et al* 2004 Progress on the modeling of liquid metal, free surface, MHD flows for fusion liquid walls *Fusion Eng. Des.* **72** 3–34

[2] Jaworksi M.A. *et al* 2013 Liquid lithium divertor characteristics and plasma-material interactions in NSTX high performance plasmas *Nucl. Fusion* **53** 083023

[3] Rhoads J.R. *et al* 2014 Effects of magnetic field on the turbulent wake of a cylinder in free-surface magnetohydrodynamic channel flow *J. Fluid Mech.* **742** 446

[4] Rhoads J.R. 2013 *Magnetohydrodynamics and Heat Transfer in a Free-Surface, Flowing Liquid Metal Experiment* (Princeton, NJ: Princeton University Press)
[5] Kirillov I.R. *et al* 1995 Present understanding of MHD and heat transfer phenomena for liquid metal blankets *Fusion Eng. Des.* **27** 553
[6] Krasnov D. *et al* 2012 Numerical study of magnetohydrodynamic duct flow at high Reynolds and Hartmann numbers *J. Fluid Mech.* **704** 421
[7] Barleon L. *et al* 2001 Magnetohydrodynamic heat transfer research related to the design of fusion blankets *Fusion Technol.* **39** 127–56
[8] Cuevas S. *et al* 1997 Liquid-metal MHD flow in rectangular ducts with thin conducting or insulating walls: laminar and turbulent solutions *Int. J. Eng. Sci.* **35** 485–503
[9] Morley N.B. *et al* 2008 GaInSn usage in the research laboratory *Rev. Sci. Instrum.* **79** 056107
[10] Sahu S. *et al* 2013 COMSOL as a tool for studying magneto-hydro-dynamic effects in liquid metal flow under transverse magnetic field *COMSOL Conf. (Bangalore)* (https://researchgate.net/publication/269167920_COMSOL_as_a_tool_for_studying_Magneto-Hydro-Dynamic_effects_in_liquid_metal_flow_under_transverse_magnetic_field_Content)